# Flame Dynamics and Structure Within Sub-Millimeter Combustors

**Shaurya Prakash and Adrian D. Armijo**
Dept. of Mechanical Science and Engineering, University of Illinois at Urbana-Champaign, Urbana, IL 61801

**Richard I. Masel**
Dept. of Chemical and Biomolecular Engineering, University of Illinois at Urbana-Champaign, Urbana, IL 61801

**Mark A. Shannon**
Dept. of Mechanical Science and Engineering, University of Illinois at Urbana-Champaign, Urbana, IL 61801

*DOI 10.1002/aic.11180*
*Published online April 23, 2007 in Wiley InterScience (www.interscience.wiley.com).*

*Non-premixed methane-oxygen flame dynamics and structures confined within an alumina combustor are described. Non-stabilized, transient flame dynamics and phenomena leading to the formation of a stable edge-like flame and distinct cellular structures that take place within combustor channels of dimensions 35 mm long, 5 mm wide, and 0.75 mm high (combustor volume ~ 130 mm$^3$) are discussed. These confined flames are surveyed by measuring the external wall temperatures, high-speed and still-frame visual flame imaging, recordings of emitted acoustics from the combustor, and capturing visible, CH*, and OH* chemiluminescence through a sapphire window. The observed dynamic flame structure is an oscillating edge-like flame accompanied by ignition-extinction events that precede the formation of a stable edge-like flame and flame cells in the reaction channel. The cellular flame structures in all cases exhibit a confined tribrachial structure with a folded or extinguished rich branch while the lean branch survives.* © 2007 American Institute of Chemical Engineers *AIChE J,* 53: 1568–1577, 2007
*Keywords: alumina ($Al_2O_3$), microcombustion, edge-flame, non-premixed, methane*

## Introduction

The high energy densities provided by combusting hydrocarbon fuels has stimulated interest in recent years toward the development of micro-and mesoscale portable heat and power sources, and systems for a myriad of applications,[1–3] including high-temperature reactors.[4,5] Much advancement has been achieved in both science and technology of micro- and mesoscale heat sources through development of micro-combustors, engines, heaters, and reactors.[4–7] Despite marked progress in the nascent field of micro-and mesoscale combustion, several issues remain with regard to constructing systems that can provide predictable and controllable heat output, have wall temperatures and gradients that can be maintained, and are durable for long operation times. Previously, homogeneous combustion using premixed flames has been shown to be a cause of combustor failure at these length scales because of high flame temperatures (greater than 2000 K) in confined spaces with a large surface-area-to-volume ratio.[8,9] Relatively lower temperature devices with external wall temperatures on the order of 1500 K or less have been developed with homogeneous non-premixed flames and catalytic combustion to circumvent the problem of material failure because of cracking or melting of the combustor.[8,10–14]

This article includes Supplementary Material available from the authors upon request or via the internet at http://www.interscience.wiley.com/jpages/0001-1541/suppmat/.

Correspondence concerning this article should be addressed to M. A. Shannon at mshannon@uiuc.edu.

Previous studies have shown the importance of surface chemistry and wall temperature in sub-millimeter combustors[3,8,9,15,16] and the effect that appropriately treated alumina ($Al_2O_3$) walls can have on maintaining high hydroxyl (OH*) radical concentration in homogeneous flames to sustain gas-phase reactions.[16]

A major challenge for device integration is to maintain an optimum balance between sustaining the combustion process and maximizing the heat output. Maintaining an optimal balance at the micro- or sub-millimeter length scale is particularly difficult as the combustion process is sensitive to heat losses[17,18] because of the typically small lateral length scales in these high surface-area-to-volume ratio systems. In addition, transient effects during start up and in operation can alter the overall combustion process in contrast to the steady-state operation.[2]

Experimental observations of cellular flame structures in laminar non-premixed flames have been previously described for treated $Al_2O_3$ combustors.[8,12] Effects of radical quenching, changing fuel/oxidant ratios, diluents, Lewis numbers, fuel/oxidant contacting pattern on these cellular flame structures have also been studied experimentally.[8,11,12] Evaluation of boundary conditions such as axial heat transfer on steady-state flame structure and external wall temperature profile has also been reported.[14,19] Computational studies have shown the importance of heat transfer in these systems and have considered various conditions for thermal quenching effects in mesoscale combustor channels.[18,20]

Flame cells and thermodiffusive instabilities in combustion processes were first reported by Smithells and Ingle in 1892.[21] Investigations of cellular structures and edge-flames are more recent.[22–26] Further, it is well known that enclosing any heat source or flame in a chamber leads to the potential of heat-driven oscillations and possible acoustic emission.[27] Acoustic emission in combustion environments has been studied extensively for well over a century[8,19,25,28–32] beginning with the work of Higgins and "singing flames" in 1777.[33] Oscillatory flame behavior leading to sound emission and including periodic extinction/re-ignition phenomena in mesoscale curved ducts has been recently explored.[25] Stabilization of premixed flame structures with acoustic emission in tubes of about 1 mm diameter has also been investigated.[19] Numerical studies have also focused on onset of oscillations, stability criteria, and oscillatory flame propagation in non-premixed configurations.[34–36]

Despite this extensive body of literature, there is a paucity of experimental data on unsteady/transient, non-stabilized flames, and the resulting steady flame structure at the micro-scale that perhaps can provide some insight into how stable flames form and are maintained in confined channels. In this work, experimental description is presented of the transient behavior and steady-state flame structure of non-premixed flames confined in a sub-millimeter channel that exhibit acoustic emission before the formation of quiet, stable cellular flames. The purpose of this paper is to report on experimental observations of the non-stabilized and transient flame dynamics that eventually lead to steady-state flame structures in sub-millimeter $Al_2O_3$ combustors. The process will be described from ignition to the formation of steady-state flame cells using: still-frame and high-speed flame structure imaging, measuring the acoustic emissions that occur during the dynamic phase of these combustors, and by capturing the visible, OH*, and CH* chemiluminescence.

## Experimental

The $Al_2O_3$ non-premixed sub-millimeter or microcombustors are machined from 1 mm thick $\alpha$-phase polycrystalline alumina sheets (96% purity from McMaster-Carr). These sheets hold their mechanical integrity to 1800°C and have a melting point of 2050°C. In addition to the structural strength required at high temperature to operate these combustors, $Al_2O_3$ is chosen as the material to fabricate these combustors as it helps reduce radical quenching for key radicals, such as OH*, that can help sustain homogeneous combustion at these length scales, in contrast to other traditionally inert materials such as quartz.[16] Detailed descriptions of surface preparation to reduce radical quenching and fabrication procedures can be found elsewhere[8,16,37–39]; however, a brief review of these methods and procedures follows.

The alumina sheets are machined with a diamond-coated saw into two identical Y-shaped pieces having a width of 10 mm and length of 35 mm. A 5 mm wide, 0.375 mm deep channel is machined into the center of the two Y-pieces so that when assembled the total depth is 0.75 mm. The depth of the channel can vary by as much as 0.1 mm between different combustors. The tolerance on all other dimensions is within 0.5 mm of the nominal size. Two channels serve as the gas inlets and the remaining channel serves as the combustion channel. A slot is machined out of one of the polycrystalline alumina pieces to fit a 36 mm $\times$ 7 mm C-plane sapphire window (420 $\mu$m thick, Crystal Systems, Salem, MA). The use of sapphire maintains chemical uniformity for the combustion environment with only minor differences believed to exist between the crystal orientation of the sapphire surface and annealed crystal grains of the polycrystalline alumina surface. Figure 1 shows the different components and the assembled combustor in operation.

The importance of surface treatment and preparation has been described previously.[8,14,16] The alumina pieces are cleaned with acetone and isopropyl alcohol followed by the standard RCA-2 clean (DI $H_2O/HCl/H_2O_2$ in 4:1:1 ratio by volume) at 60°C. Next, the polycrystalline alumina and sapphire pieces are annealed in an argon atmosphere (pressure is on the order of $10^{-2}$ Torr) at 1550°C for 1 h followed by a second anneal at 1100°C in an oxygen atmosphere (pressure $\sim$ atmospheric) for 10 h. It is hypothesized that this two-step anneal process reduces surface defects and minimizes oxygen vacancies that can exist in alumina[37,40] and assists in minimizing the effects of radical quenching.[16] All components (Figure 1) are then manually aligned and sealed along the side with an Aremco 569 high-temperature ceramic adhesive (Aremco, Valley Cottage, NY). Type R thermocouples (TCs) obtained from Omega Engineering (Stamford, CT) are strategically located along the outside wall of the alumina combustor and connected to a data acquisition system to obtain external wall temperature profiles as a function of time. High purity methane ($CH_4$) and oxygen ($O_2$) gases are controlled by M100B MKS mass flow controllers, and flow through attached hoses. The entire assembly is then packed in between two 1 inch insulation layers of fibrous alumina. The exhaust and unburnt gases flow freely into the ambient air.

The flame structure is visualized by still-frame and high-speed imaging. The still-frames are captured by a Canon EOS Mark II digital camera with an attached infrared filter, and the

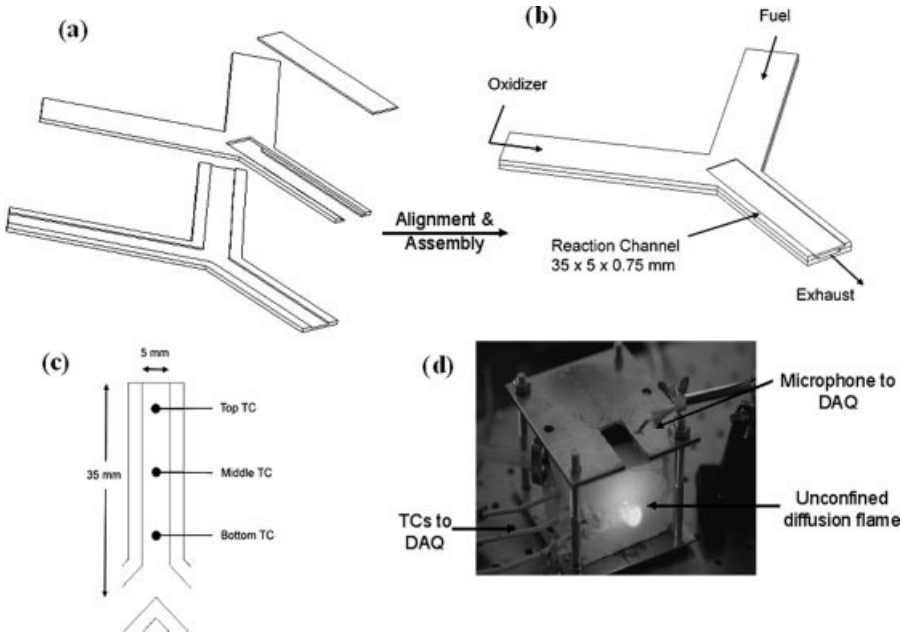


**Figure 1. Steps for the burner fabrication and operation.**

(a) An exploded view of the combustor with the sapphire window is shown. (b) The fuel and oxidizer come in at the two legs of the Y-shaped combustor, and the combustion occurs in the reaction channel as shown in the assembled combustor. The reaction channel is 5 mm wide and 35 mm long with a total depth of 0.75 mm. (c) Thermocouples are attached to the outside wall of the combustor at 0.5, 1.5, and 2 cm from the combustor exhaust. The sapphire window is not insulated for flame imaging. (d) A photograph of the windowless combustor in operation for acoustic data collection.

high-speed images are acquired by a Vision Research camera (model no. Phantom v7.1). The OH* and CH* chemiluminescence is captured using an Andor Technology iCCD camera (South Windsor, CT, Model No. DM712-18F-03). The camera settings for all intensity profiles use a 0.1 s exposure time with a gate width of 100 $\mu$s. The OH* chemiluminescence is isolated by using a narrow bandpass filter (Andover Corporation, Salem, NH) centered at 307 nm with a 10 nm bandwidth and a peak transmittance of 19%. The CH* chemiluminescence is isolated using a narrow bandpass interference filter (Edmund Optics, Barrington, NJ) centered at 430 nm with a 10 nm full-width half-maximum. The emitted sound is recorded using a Knowles Acoustic (Itasca, IL) microphone (model no. FG-3329) at a sampling rate of 20 kHz. The microphone is connected to a pre-amplifier and a Hewlett-Packard (model no. 54645D) oscilloscope to monitor the acoustic signal. In addition, the measured signal is recorded using a computer-controlled data acquisition system.

## Results and Discussion

A key to understanding the time evolution of the micro-combustion process is to observe the process from ignition to steady-state operation. The transient and non-stabilized flame structures precede the formation of a steady-state configuration. Experiments were conducted with inlet angles i.e. the included angle at which incoming gases impinge varying from 45° to 180° with no differences visually observed in the flame structures. Moreover, the $CH_4$ and $O_2$ flow rates were independently varied from 250 to 400 sccm total, with no major change observed in the flame structure, save for location of the cells. All results discussed here are for a combustor with the gases impinging on each other at an inlet angle of 90°. The total flow is laminar, with $30 < Re < 85$, and previous flow imaging observations have not shown any apparent turbulent or eddy mixing along the reaction channel,[12] which implies that the inter-diffusion of various species dominates the mixing between the fuel, oxidizer, and combustion intermediates. However, microscale flow imaging during the combustion processes has not been done, therefore, increased mixing may occur in the reacting flow region due to elevated temperatures in contrast to the room temperature conditions explored previously.[12] The acoustic (Figure 2) and imaging data shown are obtained from different combustors, since a sapphire window without insulation is needed to obtain the images. In addition, insulation is needed to protect the microphone from overheating and the optical measurements can be performed at a distance. Nonetheless, the general behaviors described are the same and are reproducible and repeatable. A detailed description of the choice and implementation of this experimental methodology can be found elsewhere.[39]

### *Imaging*

The combustor is ignited with an external spark at the exhaust. Upon ignition, a continuous edge-like flame forms near the middle in the combustor channel that is anchored at the base of the combustor inlet with an unconfined methane-air diffusion flame at the combustor exit. This unconfined diffusion flame likely consumes any unburnt fuel flowing out of the combustor. Extinguishing or externally blowing out

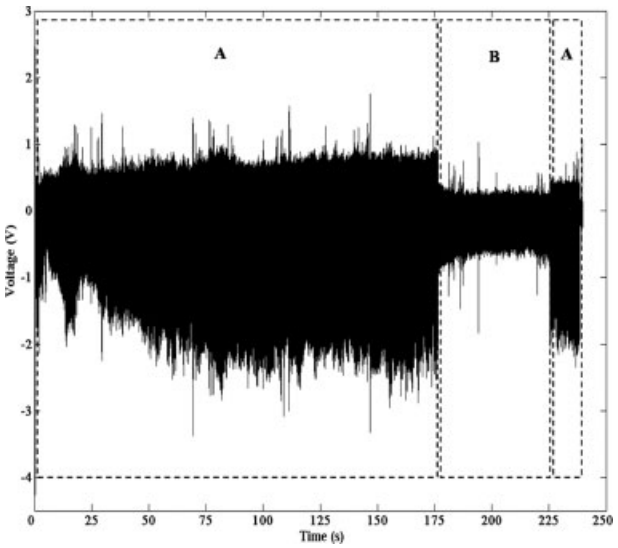


**Figure 2. A time-trace of the voltage signal from the microphone measuring the acoustic emission from the combustor.**

Regime A: A "buzzing" sound is heard indicating low frequency components. The flame imaging results corresponding to acoustic emissions are shown in Figures 3 and 4. Regime B: A "whistle" sound is heard. No sound is emitted or recorded after formation of stable flame cells (which occurs right after second Regime A). The flow conditions for this representative plot are 150 sccm of $CH_4$ and 150 sccm of $O_2$.

the external diffusion flame before the system reaches stabilization, which will be discussed later, leads to cessation of burning within the combustor channel. At early times after ignition (typically on the order of 5 s or less but for some burners has been observed to be on the order of 10 s), approximately a 1 mm wide edge-like flame is observed to both wiggle laterally (across the width of channel) and physically oscillate axially (lengthwise down the channel) within the combustor channel displaying a wavy nature as seen in the still-frame image in Figure 3a. High-speed imaging of this flame structure was carried out (Figure 3b) at 1000 frames per second with an exposure time of 900 $\mu$s. Figure 3b reveals that the wavy flame structure is not a continuous flame as depicted by still-frame imaging, but a sequence of rapidly moving individual flames. Each of these individual flames appears to be moving rapidly from the anchored edge-like flame at the combustor inlet toward the external methane-air flame at the combustor exit. The time taken for a given individual flame to travel from the anchored edge-like flame to the external diffusion flame is on the order of 7 ms which corresponds to a frequency of approximately 142 Hz.

High-speed images were also recorded to capture the process of flame stabilization. The images presented in Figure 4 were captured at 500 frames per second at an exposure time of ~1800 $\mu$s. The image sequence in Figure 4a shows that the non-stabilized and transient flame structure actually consists of a "traveling" flame cell. This cell propagates along the length of the combustor channel from the exit toward the inlet and extinguishes near the edge-like flame. It should be noted that the flame cell travels in a direction opposite to that of bulk flow $\sim$ 1.3 m/s. Laminar burning velocities for saturated hydrocarbon flames vary from 0.4 to 0.8 m/s as a function of gas-mixture composition. These velocities can increase to greater than 1 m/s with increasing flame temperature.[41–43] By contrast, the bulk flow velocity is of the same order as the laminar burning velocities for common saturated hydrocarbon flames. The ignition-extinction phenomenon of the "traveling" flame cell repeats itself at a frequency of ~62 Hz.

Initially, the combustor is ignited with an external spark and the flame travels from the combustor exit to the gas inlet forming an edge-like flame anchored at the inlet. At early times after ignition, the combustor inlet is the hottest part and the individual flames travel from the inlet to the combustor exit. In a few seconds (typically on order of 5 s) the external methane-air flame acting as a heat source warms the combustor so that combustor exit is the hottest part. Thus, the flames are now seen to travel from the combustor exit to the gas inlet. These observations are consistent with results published by other researchers who have shown that for mes-

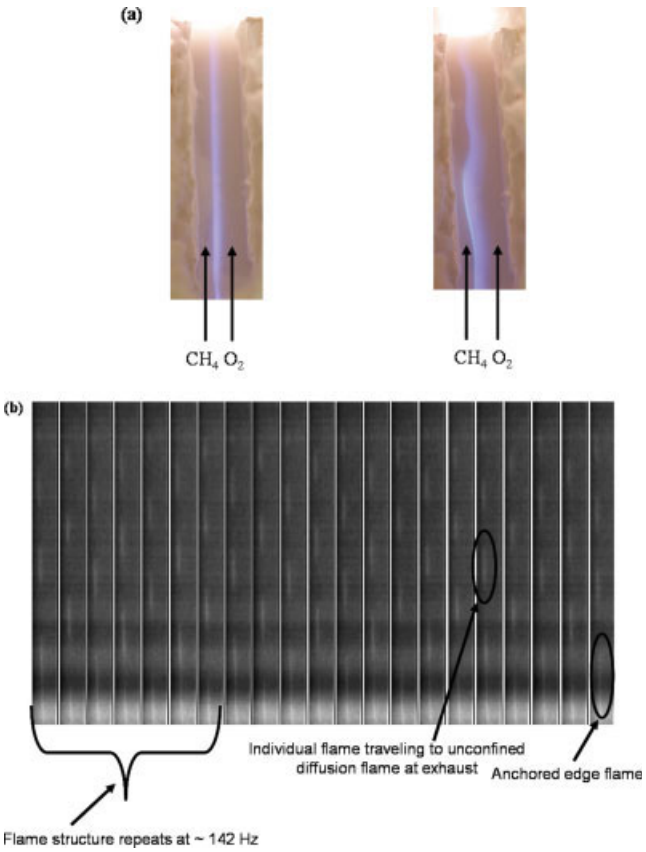


**Figure 3. Flame structure images at early times after ignition in a sub-millimeter alumina combustor.**

(a) Two different types of the transient flame structure as captured by still-frame imaging. These images lie at early times after ignition (typically less than 5 s). (b) Images from a high-speed camera corresponding to the still-frame images shown in (a) were taken at 1000 frames per second. The external methane-air diffusion flame is located at the top of the photos. Flow of fuel and oxidizer same in (b) as shown in (a). [Color figure can be viewed in the online issue, which is available at www.interscience.wiley.com.]

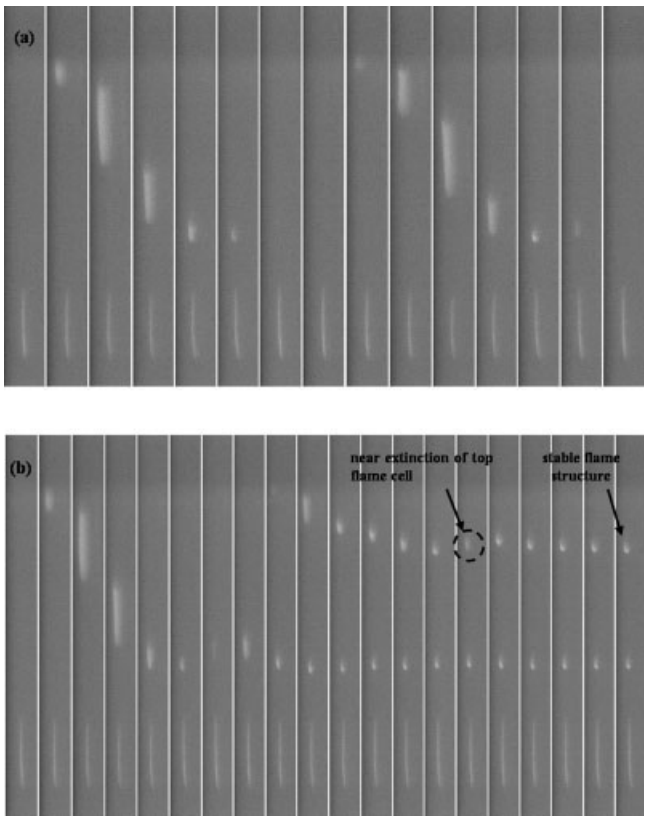


**Figure 4. High speed camera images at 500 frames per second showing in (a) the traveling flame cell, and in (b) images that capture the stabilization of the flame structure.**

oscale curved ducts re-ignition will occur at the hottest part of the duct.[25] Observations of traveling edge flames have been made by other researchers as well.[41] It can be seen from Figure 5 that the hottest part of the combustor is near the exit due to the presence of the unconfined diffusion flame that acts as a heat source and hence the ignition of the flame cells occurs near the exhaust and these flame cells travel toward the colder part of the combustor (Figure 4). This extinction-ignition phenomenon repeats itself until a steady-state is reached. High-speed imaging also shows lateral oscillations of the anchored edge-like flame at the combustor inlet at a frequency of approximately 80–90 Hz. Figure 4b depicts the process of flame stabilization (second Regime A, Figure 2) as captured via high-speed imaging, showing that first the bottom flame cell near the edge-like flame reaches stabilization followed by the top flame cell. The top flame cell stabilizes by the same ignition-extinction mechanism as the bottom flame cell. The frequency associated with the stabilization of the top flame cell is also observed to be on the order of 80 Hz as calculated from the high-speed images. The flame structure consisting of an edge-like flame and two flame cells is stable and can persist for several hours. Once the stable flame cells form, the external diffusion flame can be extinguished and the edge-like flame near the inlet and the individual flame cells remain. A description of this steady-state flame structure is presented later.

### *Acoustic emission*

The raw voltage signal obtained as a function of time from the microphone is shown in Figure 2 for a representative case of flow rate of 150 sccm each for $CH_4$ and $O_2$. In Figure 2, the acoustic signal is divided according to the type of sound heard, to be described and discussed next. However, the time in which each regime starts and/or stops changes with different combustors, flow rates of reactants, and thermal boundary conditions. Nonetheless, these distinct time regimes for the transient combustion processes are observed to occur in all cases with the general behaviors being reproducible and repeatable.

To better understand the dynamics of the observed flame structures, the frequencies being emitted during Regimes A and B, which contained notable acoustic emission, were explored. Regime A is characterized by a "buzzing" type sound comprising of low-frequency components, while Regime B is a whistle-like sound with a dominant frequency at about 700 Hz. Figure 6a is the time trace for the signal obtained 5 s after ignition (Regime A). It should be noted, as mentioned previously, that the acoustic data are for an alu-

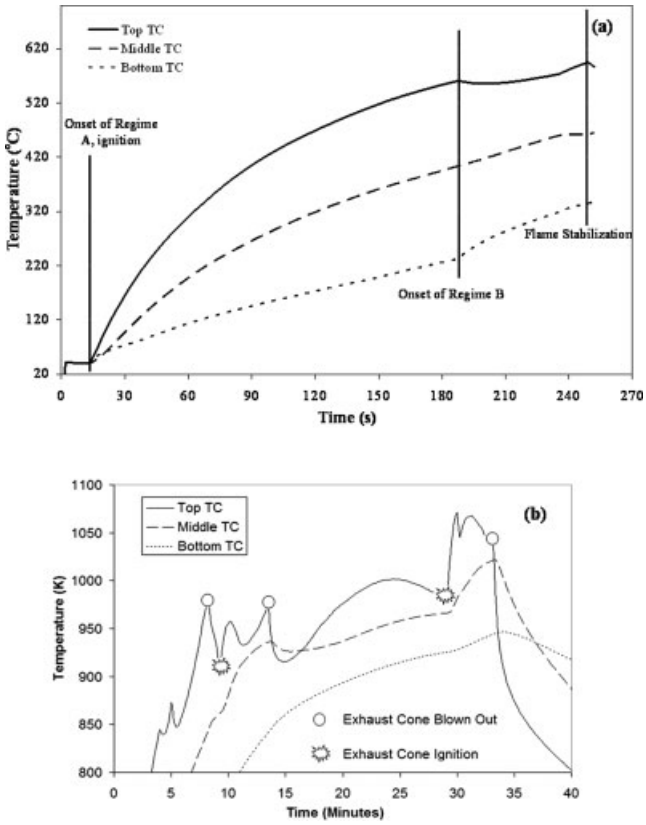


**Figure 5. (a) Representative plot showing the transient external wall temperature profile at 3 locations; (b) The external wall temperature profile for extinguishing and re-ignition of the external methane-air flame.**

In (a) thermocouples are attached as shown in Figure 1(c). The total flow rate is 300 sccm with 150 sccm each of $O_2$ and $CH_4$. The flame is ignited approximately 15 s after starting the temperature recording. Different acoustic and flame structure regimes are shown.

mina combustor without the sapphire window, which is insulated on all sides. Thus, the time taken to reach the steady-state flame configuration (also the flame stabilization state) is different from those of the sapphire window combustors used for imaging. Hence, an exact one-to-one quantitative correspondence between Figures 3, 4 and 6, 7 cannot be accomplished. However, the qualitative comparisons are still valid with the qualitative characteristics exhibited by the combustors being the same.[39,44] It can be seen in Figure 6a that the acoustic emission comprises a sharp impulse followed by three to four "ringing" type peaks. Figure 6b shows the Fast-Fourier Transform (FFT) power spectrum of time signal shown in Figure 6a. The sharp impulse followed by the ringing structure repeats itself at a frequency of ~65 Hz. This frequency is within 3 Hz of the frequency of ignition-extinction phenomenon visually observed of the traveling flame-cell shown in Figure 4. The acoustic data confirms the observation from the imaging data that there are ignition-extinction events occurring within these combustors. Figure 6c shows the FFT power spectrum for the higher frequency components likely associated with exciting fluid-structure interactions, which are discussed below.

In Regime B (185–215 s after ignition) the dominant frequency is near 712 Hz, and the harmonics of this frequency are also observed. Data collected up to 10,000 Hz (20 kHz sampling rate) does not show any other frequencies between 5000 and 10,000 Hz other than harmonics of the dominant frequency in Regime B. Acoustic data analysis indicates the presence of higher frequency components that are not directly observed from flame imaging data. To help understand why these higher frequency components are present, consider the following analysis. Earlier the combustor channel was considered as a pipe closed at one end.[39] Upon closer inspection of the data (Figure 6c) and analyzing the combustor as a pipe open at both ends, it is found that the observed frequencies lie in the range of ~1000–3000 Hz. In addition, because of the differences in the physical properties of $CH_4$ and $O_2$, the speed of sound in $CH_4$ can be greater than that in $O_2$ by almost 25%, it is expected that several different acoustic modes could be present due to the speed of sound in methane, oxygen, and products, all potentially at different temperatures. Figure 5 shows that temperature gradients of approximately 100°C/cm exist along the combustor wall. For instance, 60 s after ignition the external wall temperature difference between the top TC and bottom TC (2 cm gap) is in excess of 200°C. Moreover, substantially higher temperature gradients exist laterally from the centerline of the high-temperature combustion region to the much cooler unburnt gases on either side, which will be near the wall temperatures shown in Figure 5. Therefore, the acoustic velocity varies spatially with the gas temperature. Since standing acoustic waves within the combustor depend on the gas velocity and the size of the cavity, a large range of distinct acoustic modes can be supported within the combustor. The higher frequency (>500 Hz, Figure 6c) components are therefore likely due to standing waves that are excited by the combustion process itself.

Figure 7 shows the time trace and FFT for time 45 s after ignition in Regime A. It can be seen from Figure 7a that three sharp impulse structures are present. The FFT in this time duration shows that the dominant frequency is on the

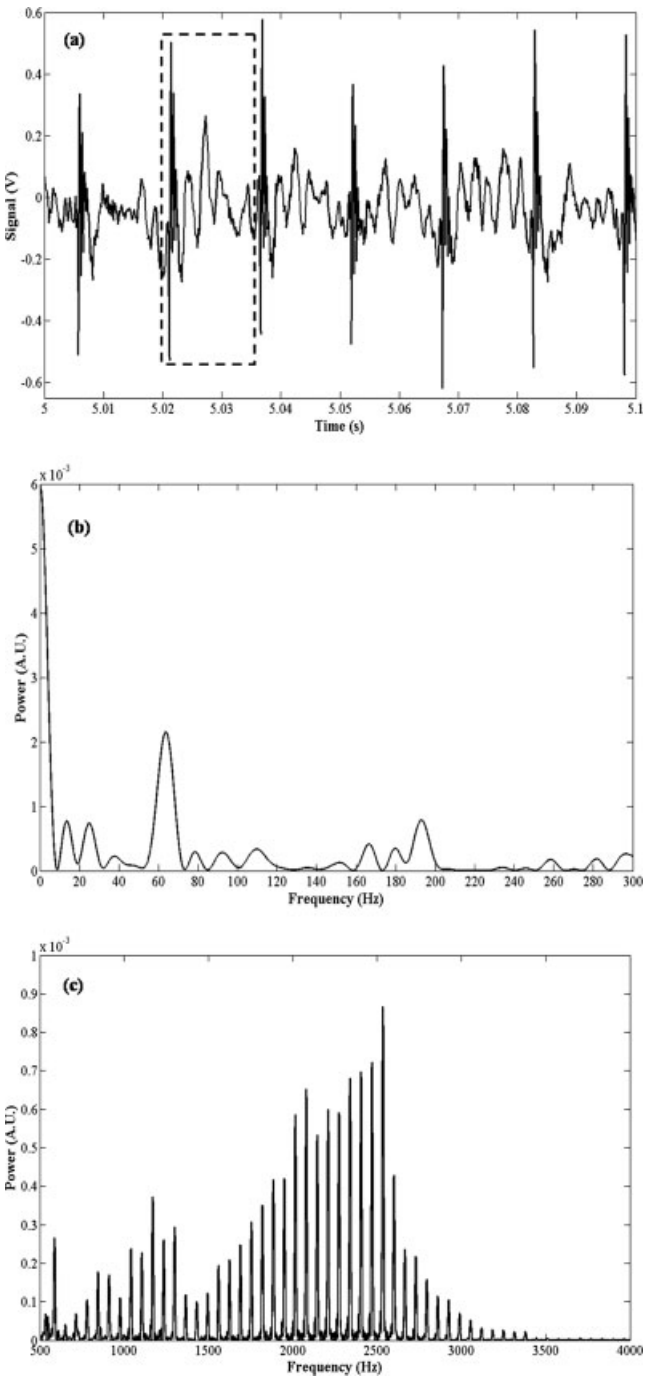


**Figure 6. (a) The plot shows a time trace for the recorded acoustic signal from 5 to 5.1 s after ignition; a sharp impulse followed by a 'ringing' type signal is observed, the signal repeats at a frequency of approximately 65 Hz; (b) the FFT of the time trace shown in (a) is seen; other frequency ranges are also observed at much weaker strengths; total flow rate: 300 sccm with equal $CH_4$ and $O_2$; (c) the FFT also shows high frequency components most likely due to the coupling between flowing gases and the combustor structure.**

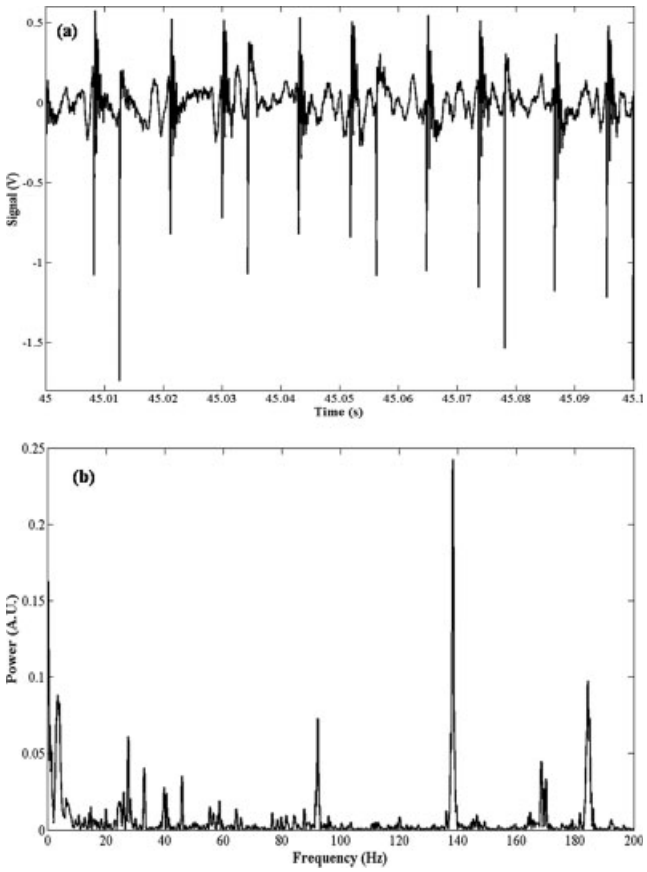


**Figure 7. (a) Time trace for 45 to 45.1 s after ignition; the acoustic data shows 3 sharp impulses; (b) FFT for the time duration 45 to 47 s after ignition showing the lower frequency components.**

The higher frequency components are similar to Figure 6(c).

order of 90 Hz and is most likely the frequency of the lateral oscillations of the anchored edge-like flame. Other frequency components observed are at ~140 Hz and ~170 Hz. A harmonic of the peak at 90 Hz is also observed near 180 Hz. The emitted frequencies during the transient flame stage can provide insight into the mechanism underlying the instabilities in the combustion process. Interestingly, it has been shown previously that the observed flame instabilities are not a strong function of non-reacting diluent gases or Lewis number.[11] Two possible types of mechanisms may be driving the instabilities in the observed combustion process: (i) hydrodynamic and (ii) thermal-diffusive. To understand which kind of instabilities can dominate the combustors discussed in this paper, a brief analysis is presented to shed some light onto the different mechanisms that can be important in these systems. To estimate if hydrodynamic instabilities may dominate, the Strouhal (St) number ($fL_c/V$, where $f$ is the frequency of oscillation, $L_c$ the characteristic length, and $V$ the velocity of flow) is estimated for each of the four dominant frequencies discussed earlier. For estimating the Strouhal number a characteristic length of 0.75 mm was used. The representative case of 150 sccm each of $CH_4$ and $O_2$ is used for the discussion here. There are two different velocities present in the microcombustors during the transient phase. These are the bulk fluid velocity directed from the combustor inlet to the exhaust and the flame velocity that is in the opposite direction (c.f. Figure 4). The bulk fluid velocity is 1.3 m/s and the relative velocity of the traveling flame cell as estimated from the high-speed images (Figure 4b) is ~2.1 m/s. For St calculations velocity of the bulk flow was used. For all frequencies examined (62, 80, 90, and 142 Hz), it was found that $0.02 < St < 0.08$. In non-reacting flows there are two ranges of St for prevalence of hydrodynamic instabilities, with typically turbulent high *Re* flows displaying hydrodynamic instabilities at $St \geq 0.2$. At low *Re*, typically laminar flows, the Strouhal number of the observed instability is in the range $0.05 < St < 0.1$; this value is typical of hydrodynamic instabilities.[45,46] However, with reacting flows such as those present here (with relatively low *Re*), large temperature gradients generally force the flows to become more stable.[46] Thus, initially the oscillations observed are caused by hydrodynamic variations in the flame propagation from strong density gradients in the gases. As the combustion process proceeds, the walls heat up above about 600 K, heating the gases up as well. The resulting coupling between the thermal and fluid fields damps out the strong hydrodynamic instabilities, and stable, steady-state flame structures result.

### *Steady-state flame structure observations*

After the end of the second Regime A, the flame dynamics cease, the acoustic emissions stop, resulting in stable flame structures. To better understand these stable flame structures, which are the end result of the dynamic initiation of the flames, the overall steady-state flame structure is described. The purpose of this section is to provide detailed experimental observations of the edge-like flame at the combustor inlet and the individual flames cells, which hopefully can help researchers develop theoretical constructs for describing the stable flame structure.

During start-up, the unconfined methane-air diffusion flame at the outlet acts as a heat source by heating the combustor wall and incoming gases from the exhaust to the inlet gas legs. During steady-state combustor operation, this unconfined methane-air diffusion flame can be extinguished, and the stable discontinuous flame structure remains within the reaction channel. When the unconfined methane-air diffusion flame is extinguished, the flame speed decreases as the combustor walls cool down,[47] causing the flame cell to travel towards the exhaust in direction of the bulk gas flow, which reignites the unconfined methane-air diffusion flame. This new methane-air diffusion flame can also be externally blown out and stable flames remain. For sapphire combustors without insulation, depending on the number of cellular flame structures that exist after start-up, this process reoccurs until only the edge-like flame at the inlet remains, and the walls cool down to a steady-state combustor wall temperature on order of 600 K. An external wall temperature profile for this process is seen in Figure 5b. The steady-state flame structure is not a traditional instability,[11] but rather a slow time varying yet stable, flame configuration that evolves with changes in wall temperature over a period of several minutes to hours, depending on the amount of insulation. The main observation is that for flame cells to stabilize within the com-

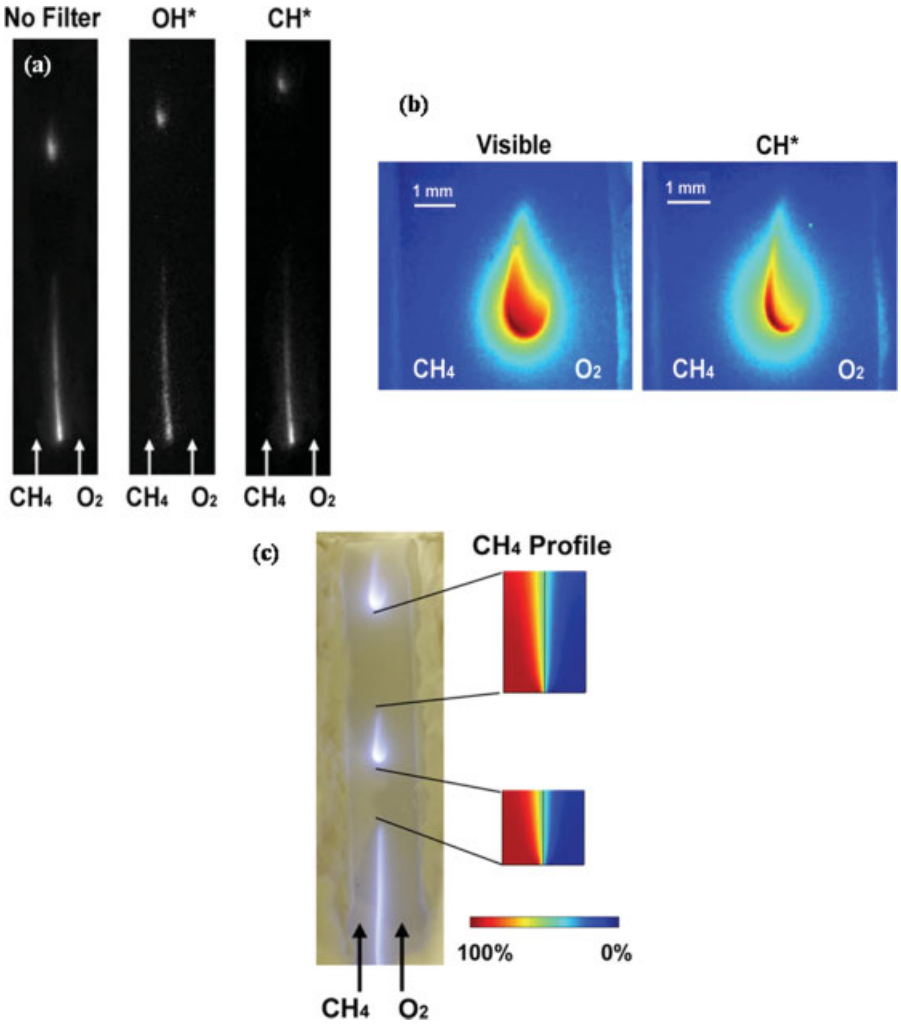


**Figure 8. (a) Relative chemiluminesence intensity profiles of the flame, OH*, and CH* taken using an intensified CCD camera; the fuel and oxidizer flow rates for these profiles are 150 sccm $CH_4$ and 150 sccm $O_2$; (b) high resolution false color chemiluminesence relative intensity profiles of the visible and CH* of the flame cell; notice the higher burning rate on the fuel-rich ($CH_4$) side in each case; the fuel and oxidizer flow rates for these photos are 100 sccm $CH_4$ and 200 sccm $O_2$; (c) the schematic illustrates the $CH_4$ spatial profile along the methane and oxygen mixing layer along the observed gaps in the flame structure.**

The fuel and oxidizer flow rates are 100 sccm $CH_4$ and 200 sccm $O_2$. The exhaust of the combustor is located at the top of the photos. [Color figure can be viewed in the online issue, which is available at www.interscience.wiley.com.]

bustor, the wall temperatures are above approximately 600 K, similar to the wall temperatures observed by other researchers for sustaining stable flames in alumina microcombustors.[3] The exact reason for the need for this specific wall temperature to sustain stable flames remains an open question, likely requiring extensive theoretical modeling to account for several coupled phenomena. These phenomena include gas-phase and surface reactions and heat transfer between the gases, combustor, and the surroundings.

To determine the extent of combustion within the microcombustor, visible and specific chemiluminescence emission lines from excited state species are imaged. The flame chemiluminescence reported here does not provide quantitative information about the combustion process; these measurements show the spatially-resolved species in the flame zone, whose concentrations are typically in proportion to the species production rates.[48] Figure 8a shows the CH* (431.1 nm) and OH* (307.1 nm) intensity profiles and the case with no filter. Each profile is internally normalized to the maximum intensity at the same point in the edge-like flame at the combustor inlet. These images are taken after the external flame is extinguished. The difference in the gap between the cellular flame structure and the inlet edge-like flame in the intensity profiles is due to slowing of the flame speed as the wall temperature cools, as discussed previously. The chemiluminescence images show that the normalized OH* profile extends over the same spatial regions as the visible flame, and the CH* profile is more confined. The extent of confinement can

be seen clearly in Figure 8b which shows high resolution false color relative intensity profiles of the visible and CH* chemiluminescence emitted by the cellular flame structure.

The shape and spacing of the flame cells is also of interest. Figure 8b demonstrates a hook-like structure, with the hook always pointing towards the direction of the oxygen flow. Figure 8c shows that the initial gap between the anchoring edge-like flame and the first flame cell is smaller by approximately 65% than the gap between two flame cells. The corresponding lateral mixing zone before the second flame cell is larger than the first by about 15%. These hook-like structures of the flame cells have been observed to occur in all cases tested under all flow conditions, fuel types, and heat transfer conditions. Why these hook-like flames have this specific shape and these intensity profiles remains an open question. One hypothesis that can explain these flame cells is that the flame zone is a laminar tribrachial (triple) flame structure. In this case, the intensity profiles imply that the rich premixed branch is either extinguished or folded onto the diffusion tail. These experimental results agree in some important respects with the numerical results of the structure and propagation of a confined triple flame.[49,50] A fuel rich flamelet for the premixed confined flame is shown to result in larger curvature and a higher burning rate flame structure.[49] The importance of the diffusion branch in the propagation of tribrachial flames was also discussed.[50] Although the present case involves a combination of partial premixing with diffusion, the methane side of the combustor is fuel rich and has a higher burning rate than the lean, oxygen rich side, as evidenced by the intensity plots (visible and CH*) in Figure 8b. McCoy et al.[51] modeled the transient behavior of an unconfined methane-air system by showing the key gas-phase radical profiles, such as CH* and OH*, which exhibited a folded flame structure of the rich phase, similar to what is observed here in the stable, time varying flame cell. Neither of these cases consider the effects of radical quenching of the walls, which can be expected to vary for the CH* and OH* radicals, and are known to strongly affect microcombustion. In addition, microchannels with laminar flows in Y-shaped channels, such as the combustors here have been shown to undergo diffusive broadening in absence of reaction. This diffusive broadening occurs as flow moves from the inlet to the exit.[52] Clearly, the observed flame structure is a result of several coupled phenomena governed by a large number of parameters and requires further investigation. The authors hope that the experimental evidence shown in the current work will motivate theoretical research that quantifiably explains the experimental observations.

## Conclusions

The experimental results show that a physically oscillating flame exists after initiation that is accompanied by numerous ignition/extinction events, which also corresponds with emitted sound. These dynamic flame events eventually lead to the formation of stable flames comprised of discrete burning zones. The fuel type and inlet mixture ratio of fuel and oxidizer, as well as the relative shear between fuel and oxidizer streams, do not appear to be the primary factors affecting flame stabilization for these non-premixed systems. The transient flame structures are strongly affected by the total flow rate. The high-speed imaging data together with the recorded acoustic signal shows that the transient flame structure is characterized by ignition-extinction events and a laterally oscillating edge flame anchored at the inlet. Multiple frequencies exist varying from low frequency components ($<$200 Hz) characteristic of the dynamics of the flames to several higher frequency components ($>$500 Hz) that are probably due to the interaction between gases and the combustor structure.

Direct imaging of the steady-state flame structure shows that two stable flame structures are observed within an alumina submillimeter combustor fed by non-premixed fuel and oxidizer: an edge-like flame that is anchored at the inlet and partially premixed cellular flame structures that occur discontinuously along the reaction channel. The anchor point is essential for maintaining stable flames downstream in the combustor where flow speeds are relatively high ($\sim$1 m/s). The stable flame cells, with or without the unconfined methane-air diffusion flame on top of the burner, only occur once the combustor walls are sufficiently hot to sustain the flame within the confined space. This flame cell structure is initially dominated by a hydrodynamic instability, which reaches a steady-state flame cell structure because of the stabilization introduced by a strong coupling between the thermal and fluid fields. The location of the flame cell(s) within the combustor is strongly dependent on the temperature of the walls and combustion gases. The anchoring edge-like flame acts to increase the temperature of the combustion gases that feed the flame cells. The flame cells have a hook-like shape with the highest intensity on the fuel rich side of the partially premixed flame, and the hook always pointing toward the lean oxidizer side. It is hoped that this experimental work will lead to the development of theoretical models that can explain the flame dynamics in greater detail and thus help develop design rules for building microcombustors.

## Acknowledgments

This work was supported by the Department of Defense Multidisciplinary University Research Initiative (MURI) program administered by the Army Research Office under grant DAAD19-01-1-0582. The authors thank Jeahyong Han, Jessica Mullen, Robert Covderdill, Prof. C.F. Lee, Prof. D.C. Kyritsis, Kowtilya Bijjula, Craig Miesse, Chaitanya Gupta, and Dillon Yoshitomi for assistance during various phases of this work.

## Literature Cited

1. Dunn-Rankin D, Leal EM, Walther DC. Personal power systems. *Prog Energy Combust Sci*. 2005;31:422–465.
2. Fernandez-Pello C. Micro-power generation using combustion: issues and approaches. *Proc Combust Inst*. 2002;29:883–899.
3. Vican J, Gajdeczko BF, Dryer FL, Milius DL, Aksay IA, Yetter RA. Development of a microreactor as a thermal source for microelectromechanical systems power generation. *Proc Combust Inst*. 2002;29:909–916.
4. Schaevitz SB, Franz AJ, Jensen KF, Schmidt MA. A combustion-based MEMS thermoelectric power generator. In: *The 11th International Conference on Solid-State Sensors and Actuators*, Munich, Germany, 2001:30–33.
5. Shannon MA, Moore GV, Ganley J, Miesse CM, Rice C, Seebauer EG, Masel RI. High-temperature microcombustion-based ammonia microchemical hydrogen generator reactors for PEM fuel cells. In: *Technical Digest Solid-State Sensors and Actuators Workshop*, Hilton Head Island, SC. 2002:27–30.
6. Ganley JC, Riechmann KL, Seebauer EG, Masel RI. Porous anodic alumina optimized as a catalyst support for microreactors. *J Catal*. 2004;227:26–32.
7. Mehra A, Zhang X, Ayon AA, Waitz IA, Schmidt MA, Spadaccini CM. A six-wafer combustion system for a silicon micro-gas turbine engine. *J Microelectromech Syst*. 2000;9:517–527.

8. Miesse CM, Masel RI, Jensen CD, Shannon MA, Short M. Submillimeter-scale combustion. *AIChE J*. 2004;50:3206–3214.
9. Moore G. Failure of a thin-film mullite synthesis due to carbothermic reduction by the SiC. Urbana, IL: Department of Mechanical and Industrial Engineering, University of Illinois, 2000.
10. Kyritsis DC, Coriton B, Faure F, Rouchoudhury S, Gomez A. Optimization of a catalytic combustor using electrosprayed liquid hydrocarbons for mesoscale power generation. *Combust Flame*. 2004;139: 77–89.
11. Miesse CM, Masel RI, Short M, Shannon MA. Diffusion flame instabilities in a 0.75 mm non-premixed microburner. *Proc Combust Inst*. 2005;30:2499–2507.
12. Miesse CM, Masel RI, Short M, Shannon MA. Experimental observations of methane-oxygen diffusion flame structure in a sub-millimetre microburner. *Combust Theor Model*. 2005;9:77–92.
13. Norton DG, Vlachos DG. Hydrogen assisted self-ignition of propane/air mixtures in catalytic microburners. *Proc Combust Inst*. 2005; 30:2473–2480.
14. Prakash S, Miesse CM, Masel RI, Shannon MA. Flame structure variations in sub-millimeter combustors due to heat transfer through combustor walls. In: *Proceedings of the Fourth Joint Meeting of the U.S. Sections of the Combustion Institute*, Philadelphia, PA, March 20–23, 2005.
15. Jensen CD. The dependence of flame/wall interactions on the composition of the walls for determining the material composition of a micro-combustor. Urbana, IL: Department of Chemical and Biomolecular Engineering, University of Illinois, 2000.
16. Prakash S, Glumac NG, Shankar N, Shannon MA. OH concentration profiles over alumina, quartz, and platinum surfaces using laser-induced fluorescence spectroscopy in low-pressure hydrogen/oxygen flames. *Combust Sci Technol*. 2005;177:793–817.
17. Aichlmayr HT. Design considerations, modeling, and analysis of micro-homogeneous charge compression ignition combustion free-piston engines. Minneapolis, MN: University of Minnesota, 2002.
18. Ronney PD. Analysis of non-adiabatic heat-recirculating combustors. *Combust Flame*. 2003;135:421–439.
19. Miller FJ, Dietrich DL, Struk P, Tien JS, Mellish BP. Premixed flames stabilized on or spreading inside microtubes. In: *Proceedings of the Fourth Joint Meeting of the U.S. Sections of the Combustion Institute*, Philadelphia, PA, March 20–23, 2005.
20. Lee DH, Kwon S. Heat transfer and quenching analysis of combustion in a micro combustion vessel. *J Micromech Microeng*. 2002;12:670–676.
21. Smithells A, Ingle H. The structure and chemistry of flames. *J Chem Soc*. 1892;61:204.
22. Buckmaster J. Edge-flames. *Prog Energy Combust Sci*. 2002;28: 435–475.
23. Daou J, Matalon M. Influence of conductive heat-losses on the propagation of premixed flames in channels. *Combust Flame*. 2002;128: 321–339.
24. Daou R, Daou J, Dold J. Effect of heat-loss on flame-edges in a premixed counterflow. *Combust Theor Model*. 2003;7:221–242.
25. Richecoeur F, Kyritsis DC. Experimental study of flame stabilization in Low Reynolds and Dean Number flows in curved mesoscale ducts. *Proc Combust Inst*. 2005;30:2419–2427.
26. Buckmaster J, Weber RO. Edge flame holding. *Proc Combust Inst*. 1996;26:1143–1149.
27. Raun RL, Beckstead MW, Finlinson JC, Brooks KP. A review of Rijke tubes, Rijke burners and related devices. *Prog Energy Combust Sci*. 1993;19:313–364.
28. Feldman KT Jr. Review of the literature on Sondhauss thermoacoustic phenomena. *J Sound Vib*. 1968;7:71–82.
29. Feldman Jr. KT. Review of literature in Rijke thermoacoustic phenomena. *J Sound Vib*. 1968;7:83–89.
30. Nicoud F, Poinso T. Thermoacoustic instabilities: should the Rayleigh criterion be extended to include entropy changes? *Combust Flame*. 2005;142:153–159.
31. Rayleigh JWS. The explanation of certain acoustical phenomena. *Nature*. 1878;18:319–321.
32. Gonzalez M. Acoustic instability of a premixed flame propagating in a tube. *Combust Flame*. 1996;107:245–259.
33. Tyndal J. *Sound*. New York: D. Appleton & Company, 1897.
34. Thatcher RW, Dold JW. Edges of flames that do not exist: flame-edge dynamics in a non-premixed counterflow. *Combust Theor Model*. 2000;4:435–457.
35. Thatcher RW, Omon-Arancibia AA, Dold JW. Oscillatory flame edge propagation, isolated flame tubes and stability in a non-premixed counterflow. *Combust Theor Model*. 2002;6:487–502.
36. Kukuck S, Matalon M. The onset of oscillations in diffusion flames. *Combust Theor Model*. 2001;5:217–240.
37. Miesse CM. Development of microcombustors and characterization of confined sub-millimeter laminar diffusion flames. Urbana, IL: Department of Chemical and Biomolecular Engineering, University of Illinois, 2005.
38. Prakash S, Armijo AD, Masel RI, Shannon MA. Characterizing non-premixed sub-millimeter combustion. In: *The Sixth Internationational Workshop on Micro and Nanotechnology for Power Generation and Energy Conversion Applications*, Berkeley, CA. 2006:17–20.
39. Prakash S, Armijo AD, Masel RI, Shannon MA. Flame dynamics in sub-millimeter combustors. *Int J Alternative Propulsion*. 2007;1: 325–338.
40. Henrich VE, Cox PA. The Surface Science of Metal Oxides. Cambridge: Cambridge University Press, 1994.
41. Cha MS, Ronney PD. Propagation rates of nonpremixed edge flames. *Combust Flame*. 2006;146:312–328.
42. Kuo KK. *Principles of Combustion*. New York: Wiley, 1986.
43. Rozenchan H, Zhu DL, Law CK, Tse SD. Outward propagation, burning velocities, and chemical effects of methane flames up to 60 atm. *Proc Combust Inst*. 2002;29:1461–1469.
44. Prakash S, Armijo AD, Masel RI, Shannon MA. Unsteady flames in microcombustion. In: *ASME International Mechanical Engineering Congress and Exposition*, Chicago, IL, 2006.
45. Crow SC, Champagne FH. Orderly structure in jet turbulence. *J Fluid Mech*. 1971;48:547–591.
46. Wee D, Park S, Yi T, Annaswamy AM, Ghoniem AF. Reduced order modeling of reacting shear flow. In: 40th AIAA Aerospace Sciences Meeting Conference and Exhibit, Reno, Nevada, 2002.
47. Williams FA. Combustion Theory. Reading: Addison-Wesley, 1965.
48. Najm HN, Paul PH, Mueller CJ, Wyckoff PS. On the adequacy of certain experimental observables as measurements of flame burning rate. *Combust Flame*. 1998;113:312–332.
49. van Oijen JA, de Goey LPH. A numerical study of confined triple flames using a flamelet-generated manifold. *Combust Theor Model*. 2004;8:141–163.
50. Kim NI, Seo JI, Guahk YT, Shin HD. The propagation of tribrachial flames in a confined channel. *Combust Flame*. 2006;146:168–179.
51. McCoy RB, Najm HN, Ray J. Shear layer effect on edge flame structure in a non-premixed methane-air flame. In: *Proceedings of the Third Joint Meeting of the U.S. Sections of the Combustion Institute*, Chicago, Illinois, March 16–19, 2003.
52. Ismagilov RF, Stroock AD, Kenis PJA, Whitesides G, Stone HA. Experimental and theoretical scaling laws for transverse diffusive broadening in two-phase laminar flows in microchannels. *Appl Phys Lett*. 2000;76:2376–2378.

*Manuscript received Sept. 14, 2006, and revision received Mar. 9, 2007.*